ERL injector operations: an investigation of beam alignment methods in the ERL injector prototype

Bela Abolfathi

Physics Department, Reed College, Portland, OR, 97202

August 13, 2010

The startup and shutdown processes for the injector were automated using MATLAB as well as the EPICS and DOOCS environments. Two beam improvement methods were explored and implemented in the injector prototype. Injector processes were automated in order to center the laser directly at the cathode. Furthermore, in an effort to improve focusing effects prior to entering the cyromodule, a program was written to center the beam inside the two solenoids. The execution of both programs was successful, however systematic errors were experienced.

1 Introduction

Synchrotron radiation has become an important tool for studying microscopic samples. However, the desire to study objects at smaller and smaller scales requires light sources with higher brilliance [1]. This equates to creating a photon beam with a higher number of photons per area in space-momentum phase space. The extent to which the particles in the beam occupy the phase space is known as the beam emittance.

Storage rings have played a significant role in high-energy research and are the basis of today's X-ray sources [2,3]. In a storage ring, a beam of electrons orbits billions of times. During circulation, the beam emits synchrotron radiation due to transverse acceleration caused by deflection in the undulators. These perturbations increase the horizontal bunch emittance, causing the brilliance of the beam to suffer over time. Demands for brighter X-rays have led scientists to come up with a more efficient way of producing these beams.

A viable alternative to storage rings is the linear accelerator, or linac. Cornell has proposed an Energy-Recovery Linac (ERL) utilizing an existing storage ring which, once constructed, will be capable of producing very high transverse coherence and a high average brilliance. Instead of storing the electrons (as would a storage ring), it is the *energy* of the electrons that is stored in an ERL. The proposed ERL will be capable of expanding the uses of hard X-ray sources by providing beams with higher intensity. Higher intensity simply means a higher energy flux. The features of the proposed 5 GeV CW superconducting electron accelerator include a normalized beam emittance of 0.3 – 0.4 mm-mrad and an average current of 100 mA.

Topics relating to the basic design of the injector and beam requirements are discussed in Section 2. Section 3 gives a brief description of the control systems used in this project. The startup and shutdown processes are outlined in Section 4. Beam alignment methods for the cathode and the solenoid are explored in Sections 5 and 6, respectively. Finally, a summary of the results is presented in Section 7.

2 Overview of ERL injector

2.1 Design

The proposed Cornell ERL is comprised of an injector, a merger, a main linac, and a return loop. An electron bunch generated in the 15 MeV injector is sent into a linac where it is accelerated to 2.7 GeV [see Fig. 1] [4]. It then goes through a turn-around loop and is further accelerated to 5 GeV in a second linac. At this point, the beam enters the Cornell Electron Storage Ring (CESR). After a single pass through the storage ring, the beam is returned to the first linac. During this pass, it is decelerated to 2.3 GeV and the energy in the beam is put back into the linac structure. This process is repeated for the second linac, the beam energy is decreased, and it is finally terminated in the beam dump.

Overall, there is approximately 5-7 MeV of beam loss due to synchrotron radiation. The rest of the energy is recycled in the electromagnetic fields of the RF (radio frequency) cavities. This energy can then be used to accelerate future electron bunches.

The layout of the ERL injector is shown in Fig. 2. A Ytterbium-based fiber laser system operating at 500 nm and then frequency-doubled provides pulses at a rate of 50 MHz for beam emittance measurements. The repetition rate can be switched to 1.3 GHz. The laser bunches hit a DC photoemission gun containing a GaAs cathode. The gun is processed to approximately 25% above the operating voltage in order to minimize the amount of dark current (any dust on the gun electrodes is essentially burned off). Electron bunches are created at the cathode and accelerated in a DC field to $E_{\text{kin}} = 350$ keV. A normal conducting buncher RF cavity and two solenoids serve to compress and focus the bunches. The beam then enters the cryomodule where it is further accelerated to $E_{\text{kin}} = 5 - 15$ MeV by five 2-cell niobium superconducting radio frequency (SRF) cavities. After leaving the cryomodule, the beam can go through one of three diagnostic beamlines where information about its transverse and longitudinal phase space is obtained. It is finally terminated in an aluminum dump which can absorb up to 600 kW of power [5].

2.2 II. Requirements for a suitable beam

One of the chief goals in constructing the ERL is to produce an extremely coherent light source with high average brightness. This is equivalent to producing a beam with high brilliance and high intensity. Coherent radiation involves reducing the particle beam cross section in phase space, and this is done by diminishing the particle beam emittance.

The transverse parameters of the particle beam are given

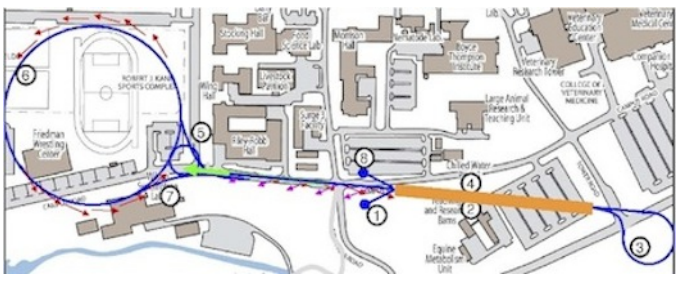

Figure 1: Layout of the Cornell's proposed ERL integrated with the Cornell Electron Storage Ring (CESR).

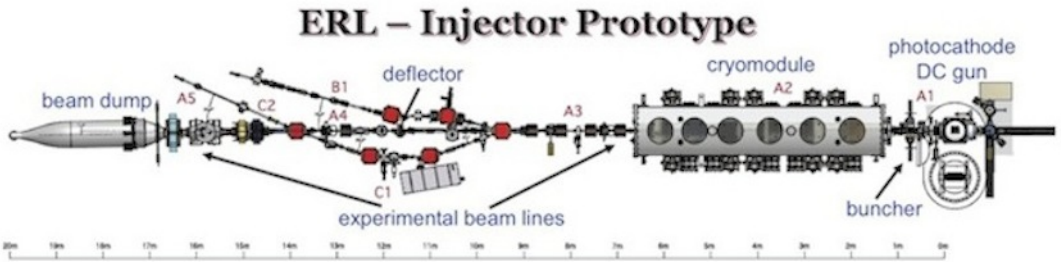

Figure 2: A diagram of the ERL injector prototype.

as a 4-dimensional vector represented by:

$$\chi(s) = \begin{pmatrix} x \\ x' \\ y \\ y' \end{pmatrix}, \tag{1}$$

where x and y are the horizontal and vertical displacements from the reference orbit, and x' and y' represent the horizontal and vertical slopes [6]. The normalized emittance $\epsilon_{x,n}$ is defined as the area occupied by the beam in phase space, and is given by the following formula:

$$\epsilon_{x,n} = \frac{p}{m_e c}\sqrt{\langle x^2\rangle\langle x'^2\rangle - \langle xx'^2\rangle^2}\ , \tag{2}$$

where p is the momentum of the beam centroid, m_e is the mass of the electron, and c is the speed of light. A pictorial representation of the transverse beam properties is provided in Fig. 3. The normalized emittance is preserved during acceleration through the linac.

The brilliance of the X-ray produced in the undulators is limited by the emittance once the beam leaves the injector. Specifically, the emittance of the beam in the linac is inherited in large part from the distribution of momenta of the electrons at the cathode of the electron gun [7]. Efforts must be made to counter emittance growth induced by space charge effects at this point in the injector. The successful operation of the ERL lies almost entirely in attaining ultra low emittance at high average current in the injector.

Failure or deficiency in any one of the injector components can restrict the brilliance or stability of the X-ray. As a result, the injector must be designed with a few key issues in mind. These include the generation of high average current, the production and preservation of high brightness electron beams, damping of higher order modes (HOMs), stable RF control of cavities operating at very high external Q (in other words, low energy loss), reduction of beam losses, and the development of precision diagnostics [8]. Table 1 provides a summary of various injector design parameters [5].

Table 1: Injector design parameters.

Parameter	Value
Nominal bunch charge	77 pC
Bunch repetition rate	1.3 GHz
Beam power	max 550 kW
Nominal gun voltage	500 kV
SC linac beam energy gain	5 – 15 MeV
Beam current	100 mA at 5 MeV
	33 mA at 15 MeV
Bunch length	0.6 mm (rms)
Transverse emittance	$<$ 1 mm-mrad

3 Control Systems

3.1 EPICS

ERL injector operations are controlled through the Experimental Physics and Industrial Control System (EPICS). EPICS interfaces to the real world with input/output controllers (IOCs). IOCs contain records which correspond to specific devices in the injector. Each record contains various fields that allow the user to access or change various components.

3.2 DOOCS

Initial steps were taken toward automating specific parts of the injector using the Distributed Object Oriented Control System (DOOCS). While fields were accessed through EPICS, several high level applications were carried out using the DOOCS environment. In addition to the programs written for DOOCS, a clean, simple interface was designed to allow for easy navigation.

Injector operations were automated so that they could be executed through DOOCS with just the click of a mouse. This was done, for example, for beam startup and shutdown processes.

During execution, status updates for each program were provided at the bottom of the window. Completion of these programs will ultimately speed up injector operations and save a substantial amount of time by allowing more time for data analysis. Automation will also improve general safety through an internal protection system by curbing problems introduced by human error.

4 Startup/Shutdown

The startup and shutdown processes were automated so that they could be executed through DOOCS with a single click of the mouse. The programs consist of list of methods that are called when the program is executed. The startup process contained a series of methods or 'status checks', beginning with a function that checks whether the L0 area is secure. Subsequent steps involved verifying that the vacuum was within the allowed range, opening the gate valves, verifying the laser settings, turning on the klystrons, turning on the buncher IOT, turning on the gun, and turning on the injector cryomodule (ICM), buncher, and deflector cavities.

The master shutdown process began with turning off the gun and was followed by turning off all ICM cavities, the buncher cavity, the deflector cavity, and the buncher IOT. This was followed by closing a gate valve and, finally, turning off the klystron high voltage (HV).

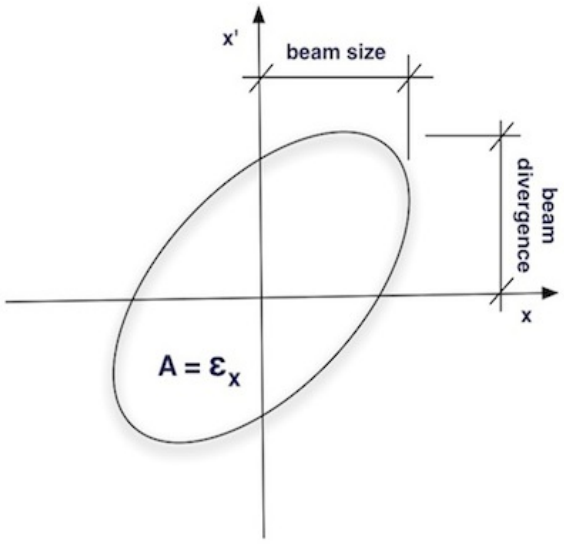

Figure 3: Phase space of the particle beam. The area is given by π times the horizontal emittance. The beam size and beam divergence are given by $\langle x^2 \rangle$ and $\langle x'^2 \rangle$ in Eq. 2.

5 Cathode Alignment

5.1 Theory

Aligning the laser beam on the cathode is a crucial step in obtaining a small emittance. The goal is to ultimately obtain a symmetric cylindrical beam. Deviation of the beam from the center of the cathode can affect its symmetry because parts of it will get focused more strongly than others. This creates a beam with larger space charge induced emittance growth and is therefore more elliptical in shape.

5.2 Methods

A section of the injector is shown in Fig. 4. The laser comes in perpendicular to the injector and is reflected off a mirror. It hits the cathode, causing electrons to accelerate through a pinhole in the anode which is held at 350 kV relative to the cathode.

The program for aligning the beam on the cathode began with verifying whether a screen was moved in. This must be done in order to prevent particles from damaging the electron gun. If it was not, then the screen was moved in and a horizontal motor was enabled. The motor is located at the mirror position and adjusts the beam position. The beam was first moved across the cathode in the horizontal direction according to a specified step size. The integrated charge of the beam was read at every step. Fig. 5 illustrates this process for an arbitrary initial beam position. Once the integrated charge fell below a certain threshold, it was assumed that it had reached the edge of the cathode. The maximum bunch charge value was recorded, a vertical motor was enabled, and the process was repeated in the vertical direction. Once the beam returned to its initial position, it was moved to the center of the cathode. The position, charge, and maximum charge values of the beam were printed during each iteration to ensure proper execution of the code and data was plotted for both the vertical and the horizontal motors. Finally, a flat-top Gaussian decay curve was fitted to each data set.

The coordinates of the center of the cathode were determined by subtracting the current motor position from the offset value (which is located at the center of the flat-top fit curve).

5.3 Results

Data was taken on two different days. Results for the horizontal motor from the first day are shown in Fig. 6. Results for both horizontal and vertical motors on the second day are shown in Figs. 7 – 8. The horizontal and vertical centers were calculated to be -2424 and 3053 motor steps, respectively.

5.4 Analysis

With regard to data taken on the first day, the integrated charge as a function of horizontal motor position was well approximated by the flat-top fit curve. It was fairly constant along the cathode until it hit the edge, where it began to decay.

Results from the second day showed slightly different results. Unlike the result in Fig. 6, there is a slight dip in the bunch charge curve on this day. This does not reflect an error in the program, but rather it shows that the quantum efficiency of the cathode is decreased at the center of the cathode. This was a result of high current runs from the previous day. The values for the horizontal and vertical centers were compatible with the centers shown in the graphs.

As to whether the program was properly executed, the values that were printed out at each step revealed that the code moved the beam according to the step size. Moreover, the program kept track of the maximum value for the bunch charge. The motor also reversed directions when the intensity of the beam fell below the threshold value. From an operational perspective, the execution of the code was successful. However, it is uncertain whether the beam was moved an equal distance during each step. It may have been the case that it moved more than the step size during one iteration, less the second time, etc. As a result, it is difficult to say whether the center of the cathode was in fact the 'true' center.

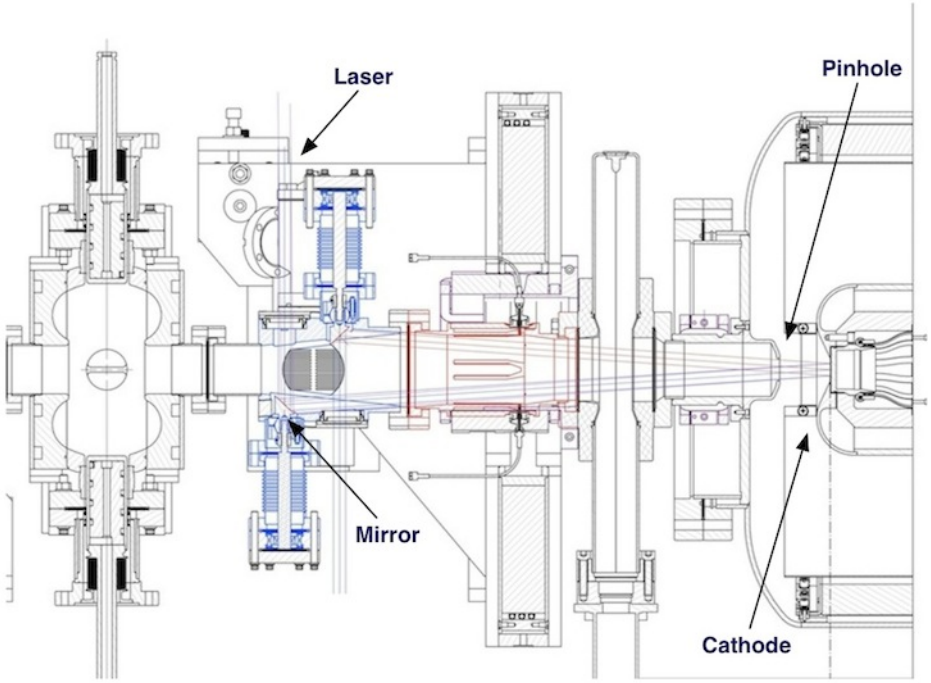

Figure 4: A section of the A1 beamline viewed from above.

6 Solenoid Alignment

6.1 Theory

Ultra low emittance is also dependent upon proper alignment of the beam with the central axis of the solenoid. The beamline for aligning the first solenoid consists of a drift space, then a solenoid, then another drift space [see Fig. 9]. If, upon entry, the trajectory of the beam is not aligned with the central axis of the solenoid, then it will be focused more strongly on one side than on the other. This will ultimately cause the emittance of the beam to suffer.

6.2 Methods

An alignment method was implemented for the first solenoidal focusing magnet in the injector (this method could be extended to the second solenoid – if assuming pure drift spaces – by accounting for the lengths of the drift spaces and the field in the solenoid).

The program extracted the transverse positions and angles of the beam at the corrector, as well as the horizontal and vertical offset of the BPM with respect to the reference trajectory of the solenoid. Subsequent correctors in the injector were turned off in order to prevent stray fields from entering the drift spaces.

The current in the corrector was adjusted for each trial, during which BPM values were obtained for a range of currents in the solenoid. The original corrector current was set to 0.080 A. It was then changed to 0.181 A in order to give the beam a vertical 'kick'. BPM values were then read once again for the original corrector current. Finally, BPM values were obtained for a corrector current of -0.181 A in order to give the beam a horizontal 'kick'. The position of the beam at the BPM was plotted for each trial. Furthermore, values for the beam positions and angles at the corrector and the BPM offset were calculated. The statistical error for each value was also derived. This was done using the algebra in the following section.

The vector describing the initial beam positions and the BPM offset can be written as:

$$\xi(s) = \begin{pmatrix} x \\ x' \\ y \\ y' \\ x_{\text{offset}} \\ y_{\text{offset}} \end{pmatrix}, \tag{3}$$

where the first four parameters are the same as in Eq. 1, and x_{offset} and y_{offset} denote the horizontal and vertical offset of the BPM with respect to the central trajectory of the solenoid.

The transport of the beam was determined using transfer matrices. The first order transfer matrix for a solenoid is given by

$$S = \begin{pmatrix} C^2 & \frac{1}{k}SC & SC & \frac{1}{k}S^2 \\ -kSC & C^2 & -kS^2 & SC \\ -SC & -\frac{1}{k}S^2 & C^2 & \frac{1}{k}SC \\ kS^2 & -SC & -kSC & C^2 \end{pmatrix}, \tag{4}$$

where $C = \cos(kL_s)$, $S = \sin(kL_s)$, L_s is the effective length of the solenoid, and $k = B_0/2B\rho_0$, where B_0 is the effective peak field inside the solenoid, and $B\rho_0$ is the magnetic rigidity of the beam. Magnetic rigidity is a measure of the momentum of a particle moving perpendicular to a magnetic field and is defined as [9]:

$$B\rho_0 = \frac{pc}{e}, \tag{5}$$

where B is the magnetic induction and ρ_0 is the radius of curvature of the particle.

The generalized transfer matrix D for the drift spaces is given as a function of the length of the drift space:

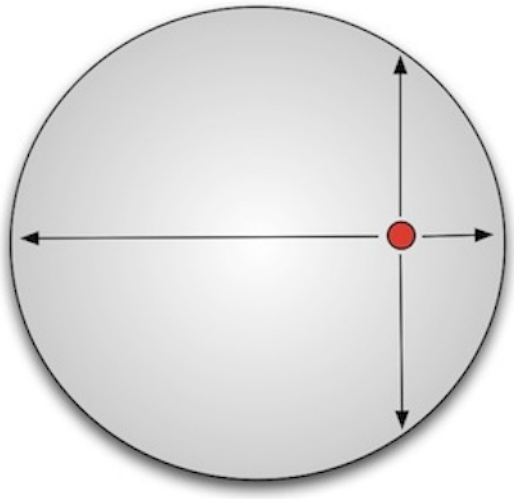

Figure 5: The cathode alignment process. The beam is shown as the red dot. It is first moved horizontally in equal step sizes until it reaches the edge of the cathode (the circular disk), and then reverses direction until it reaches the opposite edge. Bunch charge values are taken at each step. The process is repeated in the vertical direction. The center of the cathode is determined by finding the center of the fitted flat-top curve with Gaussian decay.

$$D(d) = \begin{pmatrix} 1 & d & 0 & 0 \\ 0 & 1 & 0 & 0 \\ 0 & 0 & 1 & d \\ 0 & 0 & 0 & 1 \end{pmatrix}. \tag{6}$$

The value d is the length of the drift space. The total transfer matrix M is just the product of the individual transfer matrices:

$$M = D_2 \times S \times D_1. \tag{7}$$

Since the only values that can be determined at the BPM are x and y, only the first and third rows from the transfer matrix were included in the total transfer matrix. Adding the horizontal and vertical offset, M_{T} is a 6×6 matrix with elements

$$M_{\mathrm{T}} = \begin{pmatrix} M_{11}^{(1)} & M_{12}^{(1)} & M_{13}^{(1)} & M_{14}^{(1)} & 1 & 0 \\ M_{31}^{(1)} & M_{32}^{(1)} & M_{33}^{(1)} & M_{34}^{(1)} & 0 & 1 \\ \vdots & \vdots & \vdots & \vdots & \vdots & \vdots \\ M_{11}^{(n)} & M_{12}^{(n)} & M_{13}^{(n)} & M_{14}^{(n)} & 1 & 0 \\ M_{31}^{(n)} & M_{32}^{(n)} & M_{33}^{(n)} & M_{34}^{(n)} & 0 & 1 \end{pmatrix}. \tag{8}$$

Using the weighted χ^2-method, each element of M_T is divided by the standard deviation of the horizontal and vertical positions $\langle x_i^2 \rangle$ and $\langle y_i^2 \rangle$, yielding

$$B = \begin{pmatrix} \frac{M_{11}^{(1)}}{\sigma_{x_1}} & \frac{M_{12}^{(1)}}{\sigma_{x_1}} & \frac{M_{13}^{(1)}}{\sigma_{x_1}} & \frac{M_{14}^{(1)}}{\sigma_{x_1}} & \frac{M_{15}^{(1)}}{\sigma_{x_1}} & \frac{M_{16}^{(1)}}{\sigma_{x_1}} \\ \frac{M_{31}^{(1)}}{\sigma_{y_1}} & \frac{M_{32}^{(1)}}{\sigma_{y_1}} & \frac{M_{33}^{(1)}}{\sigma_{y_1}} & \frac{M_{34}^{(1)}}{\sigma_{y_1}} & \frac{M_{35}^{(1)}}{\sigma_{y_1}} & \frac{M_{36}^{(1)}}{\sigma_{y_1}} \\ \vdots & \vdots & \vdots & \vdots & \vdots & \vdots \\ \frac{M_{11}^{(n)}}{\sigma_{x_n}} & \frac{M_{12}^{(n)}}{\sigma_{x_n}} & \frac{M_{13}^{(n)}}{\sigma_{x_n}} & \frac{M_{14}^{(n)}}{\sigma_{x_n}} & \frac{M_{15}^{(n)}}{\sigma_{x_n}} & \frac{M_{16}^{(n)}}{\sigma_{x_n}} \\ \frac{M_{31}^{(n)}}{\sigma_{y_n}} & \frac{M_{32}^{(n)}}{\sigma_{y_n}} & \frac{M_{33}^{(n)}}{\sigma_{y_n}} & \frac{M_{34}^{(n)}}{\sigma_{y_n}} & \frac{M_{35}^{(n)}}{\sigma_{y_n}} & \frac{M_{36}^{(n)}}{\sigma_{y_n}} \end{pmatrix}. \tag{9}$$

The initial beam parameters and the final transverse beam values are represented by a and b, respectively:

$$a = \begin{pmatrix} x_0 \\ x_0' \\ y_0 \\ y_0' \\ x_{\mathrm{off}} \\ y_{\mathrm{off}} \end{pmatrix}, \qquad b = \begin{pmatrix} \frac{x^{(1)}}{\sigma_{x_1}} \\ \frac{y^{(1)}}{\sigma_{y_1}} \\ \vdots \\ \frac{x^{(n)}}{\sigma_{x_n}} \\ \frac{y^{(n)}}{\sigma_{y_n}} \end{pmatrix}. \tag{10}$$

The elements in the vector b are just the final average BPM values divided by their corresponding standard deviations. These vectors are associated with the desired parameters a and the matrix B through the relation

$$B^T b = (B^T B)\, a. \tag{11}$$

Taking the inverse of the square matrix on the right hand side of Eq. 11 yields a solution for the initial beam values:

$$a = (B^T B)^{-1}\, B^T b. \tag{12}$$

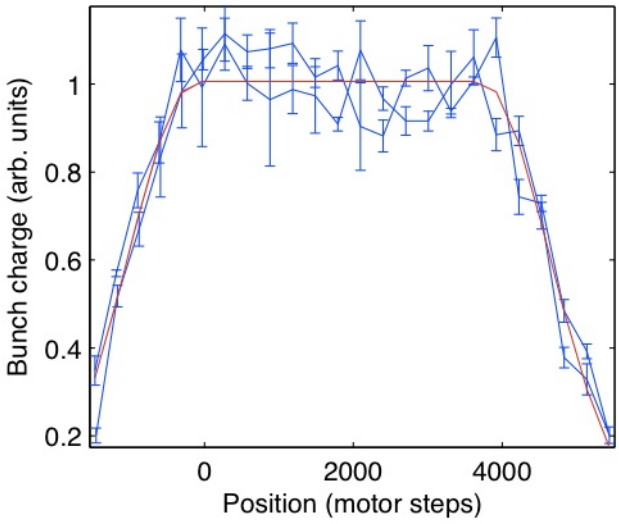

Figure 6: Bunch charge values as a function of horizontal position of the beam on the cathode taken on the first day.

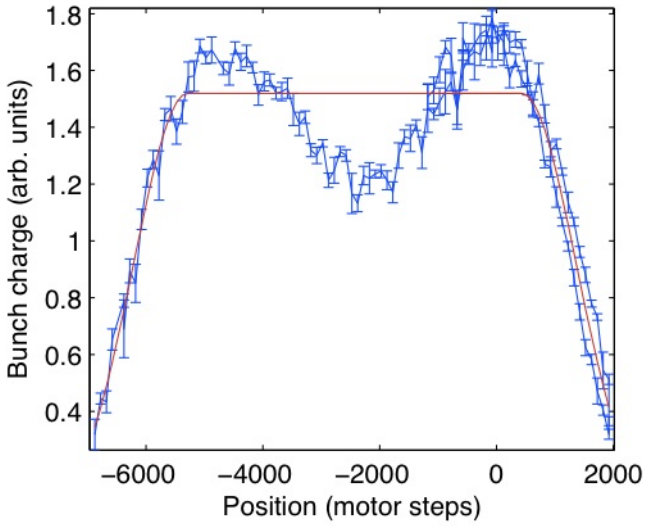

Figure 7: Bunch charge values as a function of horizontal position of the beam on the cathode taken on the second day.

Once the initial beam values are obtained, it is necessary to determine the statistical error in the calculation. The squared error of a function $f(a_1, a_2, ..., a_n)$ is given by

$$\sigma_f^2 = \sum_{i=1}^{n} \left(\frac{\partial f}{\partial x_i} \right) \sigma_{x_i}^2 + \sum_{i=1}^{n} \sum_{j=1, j \neq i}^{n} \frac{\partial f}{\partial x_i} \frac{\partial f}{\partial j_i} \mathrm{cov}(i, j). \quad (13)$$

Since there are no covariances, the squared error is given by the first expression on the right hand side of Eq. 13.

If we let $C \equiv \left(B^T B\right)^{-1}$ (from Eq. 12), then the squared errors of the searched parameters are simply the diagonals of the matrix [6]:

$$\sigma_f^2 = C = \begin{pmatrix} \sigma_{a_1}^2 & \dots & \dots & \dots & \dots & \dots \\ \dots & \sigma_{a_2}^2 & \dots & \dots & \dots & \dots \\ \dots & \dots & \sigma_{a_3}^2 & \dots & \dots & \dots \\ \dots & \dots & \dots & \sigma_{a_4}^2 & \dots & \dots \\ \dots & \dots & \dots & \dots & \sigma_{a_5}^2 & \dots \\ \dots & \dots & \dots & \dots & \dots & \sigma_{a_6}^2 \end{pmatrix}. \quad (14)$$

6.3 Results

The graphs of the BPM positions for each trial are shown in Figs. 10 – 13. Table 2 shows the calculated beam parameters at the corrector and the BPM offset values, along with the statistical error.

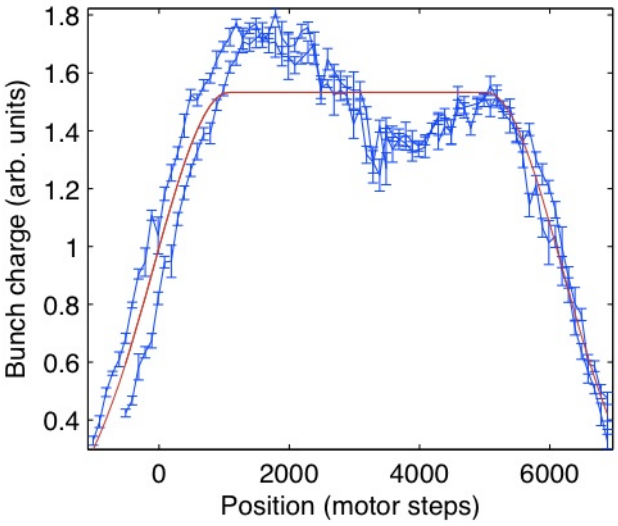

Figure 8: Bunch charge values as a function of vertical position of the beam on the cathode taken on the second day.

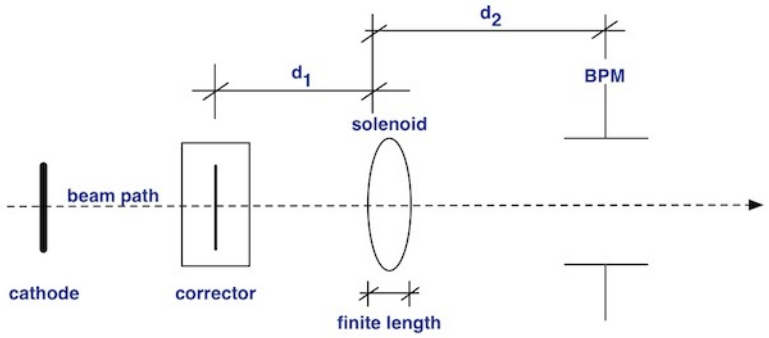

Figure 9: Schematic of the beam trajectory through the drift spaces. The beam positions are read at the BPM and used to reconstruct the initial beam values at the corrector and the BPM offset. The lengths of the drift spaces are labeled d_1 and d_2, and are the distances between the corrector and the solenoid, and the solenoid and the BPM, respectively.

6.4 Analysis

The horizontal and vertical kicks were observed in the results. The vertical kick should have theoretically increased the value of y' by 4.8 mrad, and the horizontal kick should have decreased the value of x' by -4.8 mrad. During the vertical kick, y' increased from around 4.754 mrad to 9.358 mrad, which is a difference of about 4.6 mrad. The value of x' was decreased by about 4.3 mrad as a result of the horizontal kick.

Altering the current in the corrector should not have had any affect on the other beam parameters. However, this was not the case. The values of x, y, x_{off} and y_{off} did not remain constant during each trial. Moreover, the results for Trial 1 and Trial 3 should have been identical. The statistical error is too small to account for the disparity between the expected values and the actual results alone, which leads to the conclusion that most of the error was systematic.

One possible source of systematic error is hysteresis in the magnets. Hysteresis is a common effect in ferromagnetic materials, where there is a nonlinear relationship between the magnetic field strength and the magnetic flux density. When an external magnetic field is introduced, the atomic dipoles in the material align themselves with the field. However, once the material reaches saturation and the field is removed, it retains most of its magnetization. That is, the material remains magnetized even though there is no external magnetic field.

Problems could have also been due to the BPM, specifically the dynamic range of the BPM and BPM calibration. When the beam is too close to one side of the BPM, the offset is often larger. This leads to nonlinearity in the BPM position.

Other possible sources of error are stray fields in the drifts the field integral of the solenoid. Stray fields can focus the beam in an undesirable way, and they do not have to be strong in order to have a significant affect on the beam. Since data was taken for the first solenoidal magnet, it could been the case that the field from the electron gun was contaminating the drift space(s).

Stray fields could have also been introduced by the laser moving on the cathode or from the power supply. The fieldmaps for the solenoid were calculated for a current of 1 A. However, the power supply may have not have been set to this exact value, which would alter the transfer matrix of the solenoid.

Finally, the positioning of the elements could have been a cause of systematic error. Inaccuracies in the exact mechanical and electrical centers of the elements may have affected the BPM readings.

Table 2: Initial beam values with statistical error. Values for beam parameters are shown for the original corrector current, as well as for vertical and horizontal kicks.

	Trial 1	Trial 2	Trial 3	Trial 4
	original current	vertical kick	original current	horizontal kick
x (mm)	0.588 ± 0.009	0.524 ± 0.022	0.388 ± 0.013	-0.059 ± 0.015
x′ (mrad)	1.238 ± 0.046	0.693 ± 0.080	1.718 ± 0.036	-2.500 ± 0.054
y (mm)	-1.006 ± 0.013	-1.175 ± 0.024	-0.997 ± 0.009	-0.420 ± 0.017
y′ (mrad)	4.754 ± 0.022	9.358 ± 0.100	4.147 ± 0.052	6.648 ± 0.043
x_{off} (mm)	2.815 ± 0.041	3.447 ± 0.078	2.784 ± 0.031	0.630 ± 0.047
y_{off} (mm)	-4.538 ± 0.020	-4.399 ± 0.078	-4.046 ± 0.045	-8.468 ± 0.039

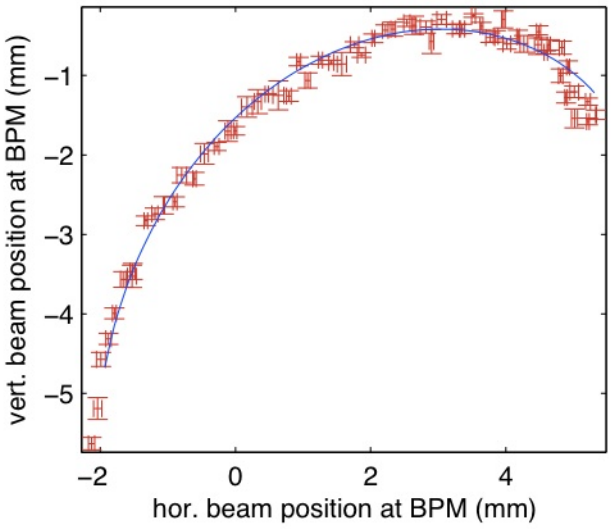

Figure 10: Trial 1: Vertical and horizontal beam positions and their respective standard deviation (denoted by red bars) at the BPM for original corrector current.

7 Conclusion

The automation of several injector procedures were written and successfully executed in the ERL injector prototype. Furthermore, two beam analysis methods were implemented in the injector. The program for aligning the cathode moved the beam and determined the center of the cathode. However it is uncertain whether this center was the 'true' center because of jumps in the motor. The method for aligning the beam along the central axis of the solenoid did not yield accurate results, and a future program should be written that takes the existence of stray fields in the drift spaces into account.

8 Acknowledgements

I would like to thank my advisors Florian Löhl and Bruce Dunham for their support and guidance during this project. I would also like to thank LEPP for allowing me to participate in this program. This work was supported by the National Science Foundation REU grant PHY-0849885 and the ERL grant DMR-0937466.

References

[1] Sol M. Gruner and Donald H. Bilderback, *Energy Recovery Linacs & Synchrotron Light Sources*, Beam Line, (2002).

[2] H. Wiedemann, *Particle Accelerator Physics I*, Springer, (2004).

[3] Georg H. Hoffstaetter, *Toward the ERL, a Brighter X-ray Source*, Cornell University.

[4] Georg H. Hoffstaetter, *ERL upgrade of an existing X-ray facility: CHESS at CESR*, Contribution to the ERL Workshop, TJNAF, (2005).

[5] Florian Löehl *Commissioning of the Cornell ERL injector*, Presentation, (2010).

[6] Florian Löehl *Measurements of the Transverse Emittance at the VUV-FEL*, (2005).

[7] Richard Talman, *Accelerator X-ray Sources*, Wiley-VCH, (2006).

[8] G.H. Hoffstaetter and B. Barstow *The Cornell ERL Prototype Project*, Proceedings of the 2003 Particle Accelerator Conference, (2003).

[9] Bruce M. Dunham *Investigations of the Physical Properties of Photoemission Polarized Electron Sources for Accelerator Applications*, (1993).

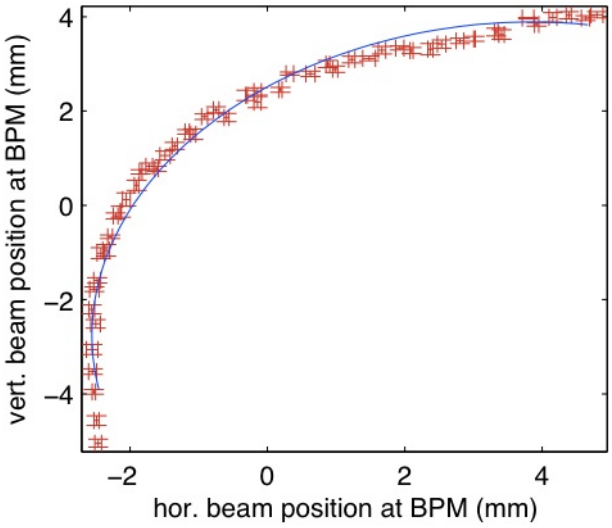

Figure 11: Trial 2: Vertical and horizontal beam positions and their respective standard deviation (denoted by red bars) at the BPM for vertical kick.

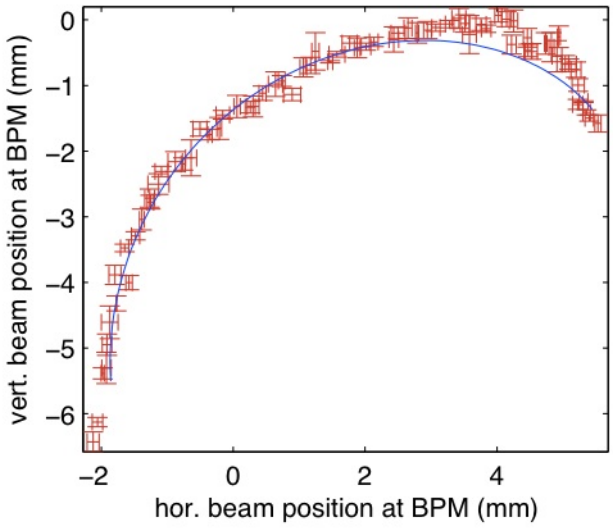

Figure 12: Trial 3: Vertical and horizontal beam positions and their respective standard deviation (denoted by red bars) at the BPM for original corrector current.

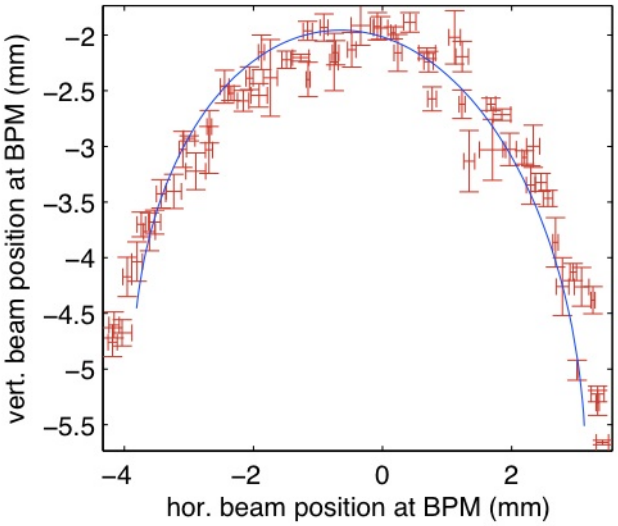

Figure 13: Trial 4: Vertical and horizontal beam positions and their respective standard deviation (denoted by red bars) at the BPM for horizontal kick.